Detecting changes in global extremes under the GLENS-SAI climate intervention strategy

Elizabeth A. Barnes[1], James Wilson Hurrell[1], and Lantao Sun[1]

[1]Colorado State University

November 24, 2022

Abstract

As anthropogenic activities continue to drive increases in extreme events, the fundamental solution of reducing greenhouse gas emissions remains elusive. Thus, there is growing interest in stratospheric aerosol injection (SAI) to offset some of the most dangerous consequences of climate change. If SAI was deployed at a global scale, it would likely be easy to detect by some metrics. However, the detectability of SAI on extreme events might be more difficult, given the presence of natural climate variability. We examine this question in climate model simulations of SAI. Specifically, we train a logistic regression model to predict whether a map of global extremes came from climate simulations with or without SAI. The timing of accurate predictions is a quantification of the time to detection of SAI impacts. We find that regional changes in extreme temperature and precipitation are robustly detected within 1 and 15 years of initial SAI injection, respectively.

Detecting changes in global extremes under the GLENS-SAI climate intervention strategy

Elizabeth A. Barnes[1], James W. Hurrell[1], and Lantao Sun[1]

[1]Department of Atmospheric Science, Colorado State University, Fort Collins, CO

Corresponding author: Elizabeth A. Barnes (eabarnes@colostate.edu)

Key Points:

- A statistical model is trained to predict whether a map of global extremes came from a RCP8.5 or stratospheric aerosol injection simulation
- The timing of accurate predictions acts as a quantification of the time to detection of a geoengineered climate
- Regional changes in extreme temperatures and extreme precipitation under SAI are robustly detected within 1 and 15 years of injection

Abstract

As anthropogenic activities continue to drive increases in extreme events, the fundamental solution of reducing greenhouse gas emissions remains elusive. Thus, there is growing interest in stratospheric aerosol injection (SAI) to offset some of the most dangerous consequences of climate change. If SAI was deployed at a global scale, it would likely be easy to detect by some metrics. However, the detectability of SAI on extreme events might be more difficult, given the presence of natural climate variability. We examine this question in climate model simulations of SAI. Specifically, we train a logistic regression model to predict whether a map of global extremes came from climate simulations with or without SAI. The timing of accurate predictions is a quantification of the time to detection of SAI impacts. We find that regional changes in extreme temperature and precipitation are robustly detected within 1 and 15 years of initial SAI injection, respectively.

Plain Language Summary

In light of concerns regarding increasing extremes driven by human-induced climate change, and the limited progress to-date of climate change solutions, a key recommendation from a recent National Academies of Science, Engineering and Medicine report is that the U.S. should establish a transdisciplinary research program into proposed climate intervention techniques, including stratospheric aerosol injection (SAI). SAI would increase the number of small reflective particles in the upper atmosphere to cool the climate by reflecting a small percentage of incoming solar radiation back into space. If SAI were deployed, the question arises as to when and where we might first detect regional impacts of SAI on climate extremes. Here, we begin to examine this question by analyzing climate model simulations of the 21st century both without and with SAI deployment. We train a simple statistical method to predict whether a map of climate extremes came from a world with or without SAI. By looking at the ability of the statistical model to accurately identify the presence (or absence) of SAI deployment, we find that regional changes in extreme temperatures and precipitation under SAI are robustly detected within 1 and 15 years of initial SAI deployment, respectively.

1 Introduction

Significant advances in the scientific understanding of climate change over the past several decades have made it clear that there has been a change in climate that goes beyond the range of natural variability (e.g., Santer et al. 2013a,b; Bonfils et al. 2020). The culprit is the astonishing rate at which greenhouse gas concentrations have increased in the atmosphere, mostly through the burning of fossil fuels and changes in land use, such as those associated with agriculture and deforestation (IPCC 2021). Greenhouse gasses are relatively transparent to incoming solar radiation while they absorb and reemit outgoing infrared radiation. The result is that more energy stays in the global climate system, raising not only temperature but also producing many other direct and indirect changes in the climate system, including changes in the frequency and intensity of extreme events (NASEM 2016).

Heat waves, for instance, are exceedingly important to human systems and infrastructure, as well as natural systems. People and ecosystems are adapted to a range of natural weather variations, but it is the extremes of weather and climate that exceed tolerances (e.g., Curtis et al. 2017; Ummenhofer and Meehl 2017). Widespread changes in temperature extremes have been observed over the last 50 years. In particular, the number of heat waves globally has increased, and there have been widespread increases in the numbers of warm nights. Cold days, cold nights and days with frost have become rarer (IPCC 2021). Changes are also occurring in the amount, intensity, frequency, and type of precipitation in ways that are also consistent with a warming planet (Trenberth et al. 2003; 2017). This includes widespread increases in heavy precipitation events and risk of flooding, even in places where total precipitation amounts have decreased (IPCC 2021).

The reality is that changes in extreme events are likely to continue for decades into the future, because of the long lifetime of CO_2 and the slow equilibration of the oceans. In other words, there is a substantial future commitment to further global climate change, even if decisive action is taken soon to reduce the global emissions of CO_2 and other greenhouse gasses. While the potential to aggressively mitigate is real, progress in realizing that potential is slow, and global greenhouse gas emissions continue at very high levels (UNEP 2021).

In light of these concerns and limited progress with solutions, including implementation of strategies to adapt to climate change impacts, research into climate intervention methods that could be used to offset the most dangerous consequences of human-induced climate change is underway (NRC 2015a,b; NASEM 2019; 2021a,b). While there are concerns over the potential adverse effects that climate intervention schemes may have (Reynolds 2019), there is a growing realization of the need to research their impacts (e.g., Keith et al. 2017).

A key recommendation from a recent National Academies of Science, Engineering and Medicine report (NASEM, 2021a) is that the U.S. should establish a transdisciplinary research program into one specific form of climate intervention - solar radiation modification (SRM) - as an important component of the nation's overall research portfolio related to climate change. A primary SRM strategy considered is stratospheric aerosol injection (SAI), which would increase the number of small reflective particles (aerosols) in the upper atmosphere to cool the climate by reflecting more incoming solar radiation away from Earth. In addition to the need to better understand the risks and benefits of SAI relative to the risks posed by climate change, the NASEM report highlighted several challenges, including our ability to detect the impacts of SAI relative to the background noise of natural climate variability. Specifically, NASEM (2021a) asked if interventions were deployed, could we confidently attribute specific climate outcomes—including extreme weather events—to the SRM intervention versus natural (unforced) variability or anthropogenic climate change? Attributing climate outcomes in the presence of natural variability is primarily a question of signal-to-noise ratio. Detection of changes in climate relative to natural climate variability and forced climate change depends on the magnitude of the climate intervention, and the spatial scales and timescales considered. It also depends on the variables considered: measuring a significant decrease in global mean temperature would likely be relatively straightforward, but measuring shifts in regional climate or the statistics of extreme events may be more difficult to detect and thus attribute.

In this paper, we begin to examine these questions by leveraging climate model simulations of climate change with and without SAI deployment. We train a simple machine learning model to predict whether a map of global extremes came from a control simulation with climate change, or a climate change simulation that includes SAI. The timing of accurate predictions acts as a quantification of the time to detection of climate intervention. We find that regional changes in extreme temperatures and precipitation under SAI are robustly detected within 1 and 15 years of initial injection, respectively.

2 Data and Methods

2.1 GLENS simulations

The Geoengineering Large-Ensemble (GLENS-SAI; Tilmes et al. 2018) is a 20-member ensemble of stratospheric sulfate aerosol geoengineering simulations between 2020-2097. It is conducted with the Community Earth System Model version 1 (Hurrell et al. 2013) with the Whole Atmosphere Community Climate Model as its atmospheric component (CESM1-WACCM; Mills et al. 2017). The climate objectives of GLENS-SAI are to maintain the global-mean surface temperature, interhemispheric surface temperature gradient, and equator-to-pole surface temperature gradient at 2020 values under the Representative Concentration Pathway 8.5 (RCP8.5) scenario (Riahi et al. 2011). Sulfur dioxide (SO_2) is injected at ~5km above the tropopause at four locations (15°N/S and 30°N/S) at each model time-step and the amount is adjusted by a feedback algorithm (MacMartin et al. 2014). The stratospheric SO_2 then oxidizes to form sulfate aerosols.

The importance of the ensemble approach arises from the presence of unpredictable natural (or internal) climate variability, which results in a range of possible outcomes for human-caused climate change (e.g., Deser et al. 2012; 2020). We compare GLENS-SAI with its corresponding RCP8.5 simulations, which include 3 members over 2010-2097 and 17 members over 2010-2030. Supp. Fig. S1 shows the global mean 1000 hPa temperature for each available ensemble member for the GLENS-SAI and RCP8.5 simulations, demonstrating the success of the GLENS-SAI simulations in keeping the global-mean temperatures at 2020 values.

2.2 Data

The main focus of this study is on extreme temperature and precipitation over land (e.g. Tye et al., 2022). Two indices are analyzed (Fig. 1): warm days (TX90p) and wet-day precipitation (R95pTOT). Following Sillmann et al. (2013a), we define TX90p to be the percentage of days when the maximum surface air temperature is above its reference 90th percentile value (centered on a 5-day window) and R95pTOT to be the annual accumulated precipitation on days when precipitation is above its reference 95th percentile value. Both indices are calculated using the 2021-2030 RCP8.5 simulation as the reference period. Additional analysis is conducted with 1000-hPa temperature and included in the supplementary materials (Supp. Fig. S1,S3,S4,S7,S10,S13).

2.3 Logistic regression architecture and training

We train a logistic regression model to take maps of extreme temperature or precipitation and predict the probability that the map came from the GLENS-SAI simulation (Supp. Fig. S2). The input maps of 45 latitude grid points by 90 longitude grid points are first flattened into a vector of size 4050 grid points prior to being fed into the model. The logistic regression model takes a multi-linear regression setup where each of the 4050 grid points acts as a predictor. The learned parameters of the model consist of 4050 weights plus a single offset ("bias") term. However, unlike standard linear regression, the sum of all of the terms is passed through the sigmoid function to rescale the output between 0 and 1. This allows us to interpret the output as a probability. A probability above 0.5 is defined as a prediction that the map came from GLENS-SAI simulation, and a probability below 0.5 is defined as a prediction that the map came from the RCP8.5 simulation.

We utilize ridge regularization (with an L_2 parameter of 0.01 for extreme temperature and 0.075 for extreme precipitation) to avoid overfitting and to ensure that the resulting maps of the regression weights are easily interpretable by eye. Our results are robust to this choice (Supp. Fig. S8, S9, S10). We train the regression weights by minimizing the binary cross-entropy loss using the Stochastic Gradient Descent (SGD) optimizer with a learning rate of 0.001 and a batch size of 32 under TensorFlow version 3.7. For the primary figures we show, we train on members #2-17 and validate on members #1, 18, 19, and 20 in both the GLENS-SAI and RCP8.5 simulations. However, due to the fact that only members #1, 2 and 3 continue beyond 2030 under RCP8.5, there is only one RCP8.5 testing member (member #1) after 2030 while there are 4 GLENS-SAI testing members. Results are robust to the combination of ensemble members used during training (Supp. Fig. S5, S6, S7).

Logistic regression is completely linear except for the final sigmoid function that scales the output between 0 and 1. We also tested simple non-linear neural network architectures but found nearly identical results to those obtained by logistic regression. Thus, we opted for the simplest prediction architecture here.

3 Results

The time series of global land averaged TX90p and relative change in R95pTOT (compared to the average 2010-2020 values under the RCP8.5 simulation) for the RCP8.5 and GLENS-SAI simulations are shown in Fig. 1a,b. Maps of the 2080-2099 ensemble mean values are shown in Fig. 1c-f. In agreement with the CMIP5 multi-model changes (Sillmann et al. 2013b), both global-mean extreme temperature and precipitation indices under RCP8.5 in CESM1 are projected to increase throughout this century under global warming. In contrast, they remain steady in GLENS-SAI, suggesting that SAI can largely offset the adverse effects from anthropogenic forcing (Fig. 1a,b). This is also the case regionally. A substantial increase in warm days is projected by the end of this century (Fig. 1c), and most of it is avoided when SAI is deployed (Fig. 1e). Likewise, extreme precipitation becomes more intense under RCP8.5 (Fig. 1d), especially in northern high-latitudes and over some regions (e.g., the Himalayas, northeast Africa and the Arabian Peninsula, and Antarctica). Such intensification largely disappears under GLENS-SAI, except over northeast Africa and the Arabian Peninsula (Fig. 1f).

Even within the first decade of simulated deployment, the number of days with extreme heat increases under the RCP8.5 forcing scenario, and GLENS-SAI reduces this increase substantially in the ensemble mean by 2030 (Fig. 2d). However, for a single given year in a single ensemble member, such forced changes are likely to be masked by natural climate variability (Fig. 2a,b), leading to more days in 2030 with extreme heat under GLENS-SAI than without (Fig. 2c). This illustrates that even if SAI acts to stabilize climate warming compared to RCP8.5, its effects on climate extremes can be masked by natural climate variability, thus potentially hinder detection efforts.

The logistic regression model, however, is able to distinguish GLENS-SAI maps of temperature extremes from those of RCP8.5 with perfect accuracy by 2025, only five years after simulated deployment (Fig. 3a). We plot the testing accuracy of the logistic regression model by showing the total number of members correctly identified for each year from 2020-2080 (Fig. 3a). Color shading denotes the percentage of ensemble members correctly identified, while the white text denotes the actual number of members correctly identified. Note that after 2030 there is only one testing member for RCP8.5 while there are four for GLENS-SAI. Even by 2021, one year after deployment, 97% or more of the temperature extreme maps across all following years are correctly identified. The logistic regression model achieves this performance by learning regional patterns (Fig. 3b,c) that act as robust indicators that distinguish the GLENS-SAI simulation from that of RCP8.5 – even in the presence of natural climate variability.

Focusing on the year 2030, a decade after initial GLENS-SAI simulated deployment, we explore which regions of the globe contribute most significantly to the logistic regression model's correct prediction of the simulation. Mean contributions are defined as the ensemble mean of the logistic regression model weights multiplied by the 2030 input maps. Put another way, for each ensemble member, each grid box's contribution is defined by that grid box's regression weight multiplied by the value of the input map at that location. Positive contributions are interpreted as regions that drive the logistic prediction toward one (i.e. toward predicting GLENS-SAI) and negative contributions are interpreted as regions that drive the logistic prediction toward zero (i.e. toward predicting RCP8.5). For the 2030 maps under GLENS-SAI (Fig. 3b), southeast Asia, Eastern Africa and Saudi Arabia, and the Eastern United States all increase the model's predicted probability that the map is from the GLENS-SAI simulation. For the 2030 maps under RCP8.5 (Fig. 3c), the eastern United States and the southern tip of South America dominate the contributions and increase the model's predicted probability that the map is from the RCP8.5 simulation (i.e. lower the probability that the map is from GLENS-SAI).

Some of the regions that act as indicators of the simulation (Fig. 3b,c) generally align with regions of high signal-to-noise ratio (Fig. 3d). Here, we define the signal as the absolute value of the ensemble mean difference between the 20 ensemble members of the GLENS-SAI and RCP8.5 simulations and the noise is defined as the range (maximum minus minimum) of the GLENS-SAI simulations in 2030 over the 20 ensemble members. However, the indicator regions are not identical to the map of signal-to-noise in part because the logistic regression model can leverage relationships *between* regions, unlike signal-to-noise which is computed gridpoint by gridpoint. In addition, the learned indicator patterns capture regions with high signal-to-noise ratio throughout the entire simulation period (not just a specific year, which can vary substantially; Supp Fig. S11) in order to distinguish an RCP8.5 world from a world with SAI.

Identifying the correct simulation using maps of extreme precipitation is a much harder task, due both to a smaller relative difference in the forced response to climate change (Fig. 1b, 4d) as well as its larger natural variability (Fig. 1b, 4a,b,c). In the case of member #1, large differences in extreme precipitation are found in 2030 between the RCP8.5 and GLENS-SAI simulations (Fig. 4c), and the majority of the differences can be attributed to natural climate variability (Fig. 4d). Even so, the logistic regression model is able to distinguish between the two simulations with nearly perfect accuracy within 15 years after simulated deployment of SAI (Fig. 5a). That is, by 2035 the model is able to correctly detect whether the precipitation extremes are occurring in a world with or without SAI in 97% or more of the maps in the years following.

As for temperature extremes, the logistic regression model learns regional patterns that act as reliable indicators of GLENS-SAI simulated deployment (Fig. 5b,c). In 2040, for instance, the regions that contribute most to the model's correct prediction of GLENS-SAI include Greenland, the Tibetan Plateau, and central Africa (Fig. 5b). That is, extreme precipitation anomalies in these regions act as indicators of simulated SAI deployment. For the 2040 maps under RCP8.5, these same regions are also the main contributors to the model's correct prediction (Fig. 5c). Extreme precipitation under RCP8.5 exhibits large increases over Central Africa (Fig. 1d), where the signal-to-noise ratio is also large (Fig. 5d; Alamou et al. 2022), and this appears to translate to large contributions to the logistic regression model's predictions (Fig. 5b,c). The same holds for Alaska and Greenland. Over most global land, GLENS-SAI exhibits little-to-no change in extreme precipitation following SAI deployment, demonstrating the success of the controller in stabilizing the climate to 2020 temperatures. One notable exception is the large ensemble-mean increase in extreme precipitation over Egypt and Libya. Note that the logistic regression model does not highlight this region as an important indicator. This is due to the fact that a similar change is seen under RCP8.5 (Fig. 1d,f).

4 Discussion & Conclusions

It is well established that, for time horizons of several decades into the future, the dominant source of uncertainty in model projections of future, regional climate is natural variability: those fluctuations in climate that occur even if there are no changes in the radiative ("external") forcing of the planet (Hawkins and Sutton 2009). Deser et al. (2012; 2020), for instance, have used large ensembles of simulations with climate models to show that natural variability can dominate regional changes in seasonal-mean temperature and precipitation over the coming decades. Similarly, Keys et al. (2022) show that the signal of SAI forcing can be strongly masked by natural variability over large regions of the globe. The presence of natural climate variability has thus been a challenge for studies attempting to detect regional climate changes due to external forcing. This problem is exacerbated further when climate extremes are considered, even though changes over time in temperature and precipitation extremes are often connected to simultaneous changes in large-scale mean temperature and atmospheric moisture content (Seneviratne et al. 2021).

Because of such challenges, it has been anticipated that it would be difficult to detect the influence of SAI on climate extremes until many decades after a hypothetical SAI deployment (NASEM 2021a). We have begun to test this assumption by tasking a simple machine learning model, a logistic regression model, with predicting whether maps of temperature and precipitation extremes came from a RCP8.5 climate change simulation or from a simulation under RCP 8.5 but with a simulated SAI deployment. We find that the logistic regression model is able to accurately detect the global impacts of SAI in temperature and precipitation extremes within 1 and 15 years, respectively. Although we train the logistic regression model using maps from many GLENS ensemble members, the logistic regression model only takes as input a single annual map at a time, and so, it must learn the regional fingerprints of SAI that distinguish it from the RCP8.5 simulation amidst a background of natural climate variability. Our approach is thus more than a gridpoint by gridpoint signal-to-noise calculation, which can vary depending on which time period and simulation is used to define the signal and which is used to define the noise (Fig. S11, S12). Instead, by framing SAI impact detection as a prediction problem over many years of data, we leverage time-evolving, regional combinations of the signal to best identify the timing of identifiable SAI impacts.

Finally, we caution that our results apply to only a single scenario of SAI forcing: the GLENS-SAI experiments performed with CESM1 (Tilmes et al. 2018). The setup of GLENS-SAI requires steadily increasing sulfur injections to counteract the RCP 8.5 forcing from continually increasing greenhouse gas concentrations in order to keep the climate at 2020 conditions. The purpose of this setup was not to suggest a realistic application, but to identify the side effects, risks, and limitations of SAI forcing. Future work will be to examine the detection of climate extremes under different SAI scenarios, including ones with more modest levels of both greenhouse gas and sulfate aerosol forcing, as well as exploring detection of regional signals which may require more complex machine learning approaches.

Acknowledgements

Work was supported, in part, by NSF CAREER AGS-1749261 (EAB) under the Climate and Large-scale Dynamics program, DARPA grant HR00112290071 (EAB, JWH), and the LAD Climate Fund (JWH).

Data Availability

All GLENS data used here is archived via the Earth System Grid (see information at www.cesm.ucar.edu/projects/community-projects/GLENS/). Code is available on github at https://github.com/eabarnes1010/actm-sai-csu/tree/main/research/glens_detection and will be archived via a permament DOI on Zenodo.

References

Alamou, E. A., J. E. Zandagba, E. I. Biao, E. Obada, C. Y. Da-Allada, F. K. Bonou, Y. Pomalegni, E. Baloitcha, S. Tilmes, and P. J. Irvine. 2022. "Impact of Stratospheric Aerosol Geoengineering on Extreme Precipitation and Temperature Indices in West Africa Using GLENS Simulations." Journal of Geophysical Research 127 (9). https://doi.org/10.1029/2021jd035855.

Bonfils, Céline J. W., Benjamin D. Santer, John C. Fyfe, Kate Marvel, Thomas J. Phillips, and Susan R. H. Zimmerman. 2020. "Human Influence on Joint Changes in Temperature, Rainfall and Continental Aridity." Nature Climate Change 10 (8): 726–31.

Curtis, S., Fair, A., Wistow, J. et al. Impact of extreme weather events and climate change for health and social care systems. Environ Health 16, 128 (2017). https://doi.org/10.1186/s12940-017-0324-3

Deser C, Phillips A, Bourdette V, Teng H (2012) Uncertainty in climate change projections: the role of internal variability. Climate dynamics, 38(3–4):527–546.

Deser, C., Lehner, F., Rodgers, K. B., Ault, T., Delworth, T. L., DiNezio, P. N., Fiore, A., Frankignoul, C., Fyfe, J. C., Horton, D. E., Kay, J. E., Knutti, R., Lovenduski, N. S., Marotzke, J., McKinnon, K. A., Minobe, S., Randerson, J., Screen, J. A., Simpson, I. R., & Ting, M. (2020). Insights from earth system model initial-condition large ensembles and future prospects. Nature Climate Change, 10(4), 277–286. https://doi.org/10.1038/s41558-020-0731-2

Hawkins, E. & Sutton, R. The potential to narrow uncertainty in regional climate predictions. Bull. Am. Meteorol. Soc. 90, 1095–1108 (2009).

Hurrell, J. W., Holland, M. M., Gent, P. R., Ghan, S., Kay, J. E., Kushner, P. J., Lamarque, J.-F., Large, W. G., Lawrence, D., Lindsay, K. (2013) The community earth system model: a framework for collaborative research. Bull. Am. Meteorol. Soc. 94, 1339–1360.

IPCC, 2021: Climate Change 2021: The Physical Science Basis. Contribution of Working Group I to the Sixth Assessment Report of the Intergovernmental Panel on Climate Change [Masson-Delmotte, V., P. Zhai, A. Pirani, S.L. Connors, C. Péan, S. Berger, N. Caud, Y. Chen, L. Goldfarb, M.I. Gomis, M. Huang, K. Leitzell, E. Lonnoy, J.B.R. Matthews, T.K. Maycock, T. Waterfield, O. Yelekçi, R. Yu, and B. Zhou (eds.)]. Cambridge University Press, Cambridge, United Kingdom and New York, NY, USA, In press, doi:10.1017/9781009157896.

Keith, D., Wagner, G. & Zabel, C. Solar geoengineering reduces atmospheric carbon burden. Nature Clim Change 7, 617–619 (2017). https://doi.org/10.1038/nclimate3376

Keys, Patrick, Elizabeth Barnes, Noah Diffenbaugh, James Hurrell, and Curtis Bell (2022). Potential for Perceived Failure of Stratospheric Aerosol Injection Deployment, submitted. Preprint available at EarthArXiv. arXiv. https://doi.org/10.31223/x5805s.

MacMartin, D. G., Kravitz, B., Keith, D. W., & Jarvis, A. (2014). Dynamics of the coupled human-climate system resulting from closed-loop control of solar geoengineering. Climate Dynamics, 43, 243–258.

Mills M. J. , J. H. Richter, S. Tilmes, B. Kravitz, D. MacMartin, S. Glanville, A. Schmidt, J. J. Tribbia, A. Gettelman, C. Hannay, J. T. Bacmeister, D. E. Kinnison, F. Vitt, and J. F. Lamarque (2017) Radiative and chemical response to interactive stratospheric aerosols in fully coupled CESM1(WACCM), JGR-Atmospheres. https://doi.org/10.1002/2017JD027006.

National Research Council, 2015a: Climate Intervention: Carbon Dioxide Removal And Reliable Sequestration. Washington, DC: The National Academies Press.https://doi.org/10.17226/18805.

National Research Council, 2015b: Climate Intervention: Reflecting Sunlight to Cool Earth. Washington, DC: The National Academies Press.https://doi.org/10.17226/18988.

National Academies of Sciences, Engineering, and Medicine, 2016. Attribution of extreme weather events in the context of climate change. National Academies Press.

National Academies of Sciences, Engineering, and Medicine, 2019: Negative Emissions Technologies and Reliable Sequestration: A Research Agenda. Washington, DC: The National Academies Press. https://doi.org/10.17226/25259.

National Academies of Sciences, Engineering, and Medicine, 2021a. ReflectingSunlight: Recommendations for Solar Geoengineering Research and ResearchGovernance. Washington, DC: The National Academies Press.https://doi.org/10.17226/25762.

National Academies of Sciences, Engineering, and Medicine, 2021b. A Research Strategy for Ocean-based Carbon Dioxide Removal and Sequestration. Washington,DC: The National Academies Press. https://doi.org/10.17226/26278.

Reynolds J. L. (2019). Solar geoengineering to reduce climate change: a review of governance proposals. Proceedings. Mathematical, physical, and engineering sciences, 475(2229), 20190255. https://doi.org/10.1098/rspa.2019.0255

Riahi, K., Rao, S., Krey, V. et al. RCP 8.5—A scenario of comparatively high greenhouse gas emissions. Climatic Change 109, 33 (2011). https://doi.org/10.1007/s10584-011-0149-y

Santer, Benjamin D., Jeffrey F. Painter, Carl A. Mears, Charles Doutriaux, Peter Caldwell, Julie M. Arblaster, Philip J. Cameron-Smith, et al. (2013a). “Identifying Human Influences on

Atmospheric Temperature.” Proceedings of the National Academy of Sciences of the United States of America 110 (1): 26–33.

Santer, Benjamin D., Jeffrey F. Painter, Céline Bonfils, Carl A. Mears, Susan Solomon, Tom M. L. Wigley, Peter J. Gleckler, et al. (2013b). “Human and Natural Influences on the Changing Thermal Structure of the Atmosphere.” Proceedings of the National Academy of Sciences of the United States of America 110 (43): 17235–40.

Seneviratne, S.I., X. Zhang, M. Adnan, W. Badi, C. Dereczynski, A. Di Luca, S. Ghosh, I. Iskandar, J. Kossin, S. Lewis, F. Otto, I. Pinto, M. Satoh, S.M. Vicente-Serrano, M. Wehner, and B. Zhou, 2021: Weather and Climate Extreme Events in a Changing Climate. In Climate Change 2021: The Physical Science Basis. Contribution of Working Group I to the Sixth Assessment Report of the Intergovernmental Panel on Climate Change [Masson-Delmotte, V., P. Zhai, A. Pirani, S.L. Connors, C. Péan, S. Berger, N. Caud, Y. Chen, L. Goldfarb, M.I. Gomis, M. Huang, K. Leitzell, E. Lonnoy, J.B.R. Matthews, T.K. Maycock, T. Waterfield, O. Yelekçi, R. Yu, and B. Zhou (eds.)]. Cambridge University Press, Cambridge, United Kingdom and New York, NY, USA, pp. 1513–1766, doi:10.1017/9781009157896.013.

Sillmann, J., Kharin, V. V., Zhang, X., Zwiers, F. W., and Bronaugh, D. (2013a), Climate extremes indices in the CMIP5 multimodel ensemble: Part 1. Model evaluation in the present climate, J. Geophys. Res. Atmos., 118, 1716– 1733, doi:10.1002/jgrd.50203.

Sillmann, J., Kharin, V. V., Zwiers, F. W., Zhang, X., and Bronaugh, D. (2013b), Climate extremes indices in the CMIP5 multimodel ensemble: Part 2. Future climate projections, J. Geophys. Res. Atmos., 118, 2473– 2493, doi:10.1002/jgrd.50188.

Tilmes, S., J.H. Richter, B. Kravitz, D.G. MacMartin, M.J. Mills, I.R. Simpson, A.S. Glanville, J.T. Fasullo, A.S. Phillips, J. Lamarque, J. Tribbia, J. Edwards, S. Mickelson, and S. Gosh (2018) CESM1(WACCM) Stratospheric Aerosol Geoengineering Large Ensemble (GLENS) Project. Bull. Amer. Meteor. Soc., https://doi.org/10.1175/BAMS-D-17-0267.1.

Trenberth, K. E., A. Dai, R. M. Rasmussen and D. B.Parsons, 2003: The changing character of precipitation.Bull. Amer. Meteor. Soc., 84, 1205-1217. https://doi.org/10.1175/BAMS-84-9-1205

Trenberth, K. E., Y. Zhang and M. Gehne, 2017:Intermittency in precipitation: duration, frequency,intensity, and amounts using hourly data. J. Hydrometeor.18, 1393-1412, Doi: 10.1175/JHM-D-16-0263.

Tye, M. R., Dagon, K., Molina, M. J., Richter, J. H., Visioni, D., Kravitz, B., Tebaldi, C., and Tilmes, S. 2022: Indices of Extremes: Geographic patterns of change in extremes and associated vegetation impacts under climate intervention, EGUsphere [preprint], https://doi.org/10.5194/egusphere-2022-1.

Ummenhofer CC, Meehl GA. Extreme weather and climate events with ecological relevance: a review. Philos Trans R Soc Lond B Biol Sci. 2017 Jun 19;372(1723):20160135. doi: 10.1098/rstb.2016.0135. PMID: 28483866; PMCID: PMC5434087.

United Nations Environment Programme (2021). Emissions Gap Report 2021: The Heat Is On – A World of Climate Promises Not Yet Delivered. Nairobi. https://www.unep.org/resources/emissions-gap-report-2021

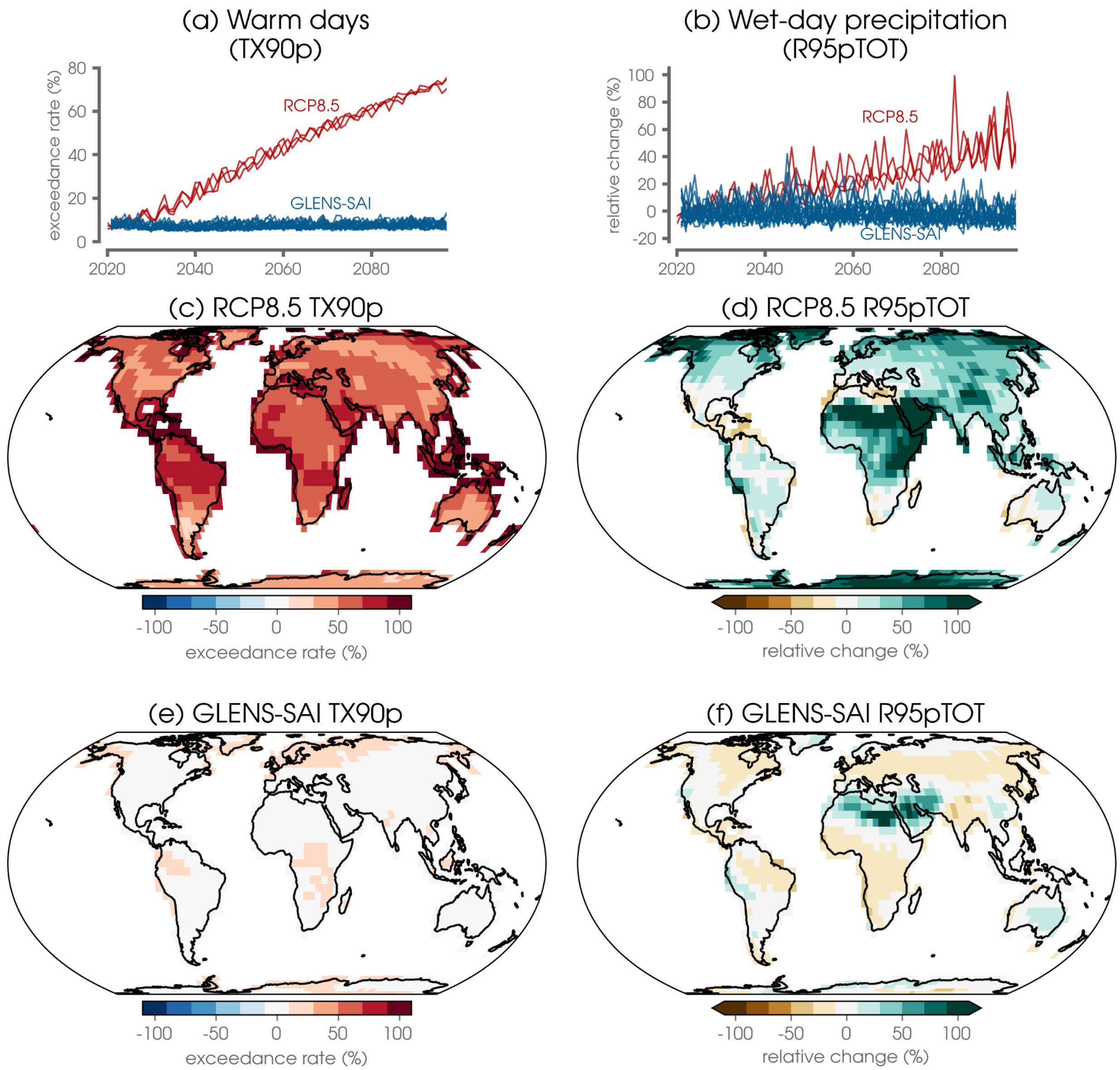

Figure 1: (a) Time series of global-mean warm days (TX90p) and (b) relative change in wet-day precipitation (R95pTOT). Relative change in wet-day precipitation is defined as the percentage change relative to the average 2010-2020 values under the RCP8.5 simulation. (c,d) Anomalous warm days and relative change in wet-day precipitation averaged over 2080-2089 in the RCP8.5 simulations. (e,f) As in (c,d) but for the GLENS-SAI simulations.

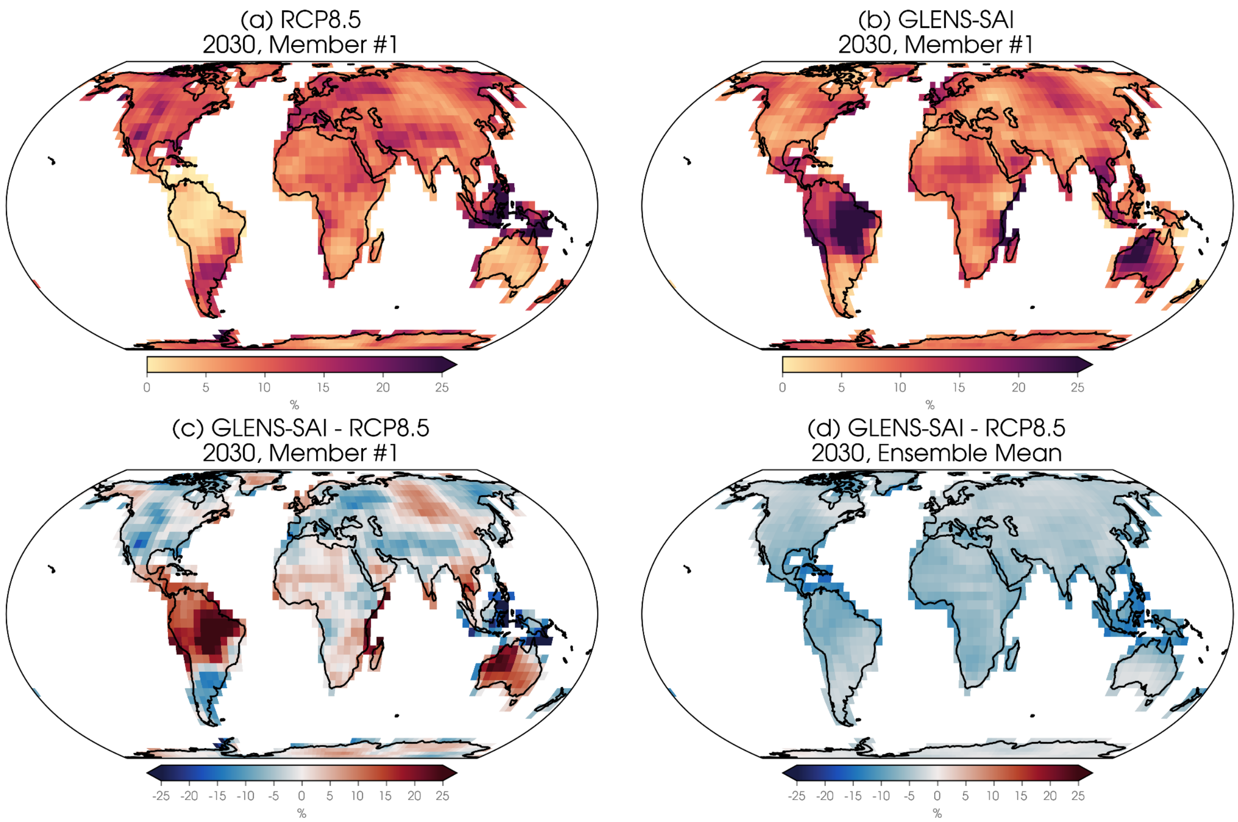

Figure 2: TX90p. Percent of days in 2030 with extreme heat for ensemble member #1 of the (a) RCP8.5 and (b) GLENS-SAI simulations. (c) The difference in the percent of days with extreme heat between GLENS-SAI and RCP8.5 for ensemble member #1. (d) As in panel (c) but for the difference in the ensemble means (20 members for each simulation).

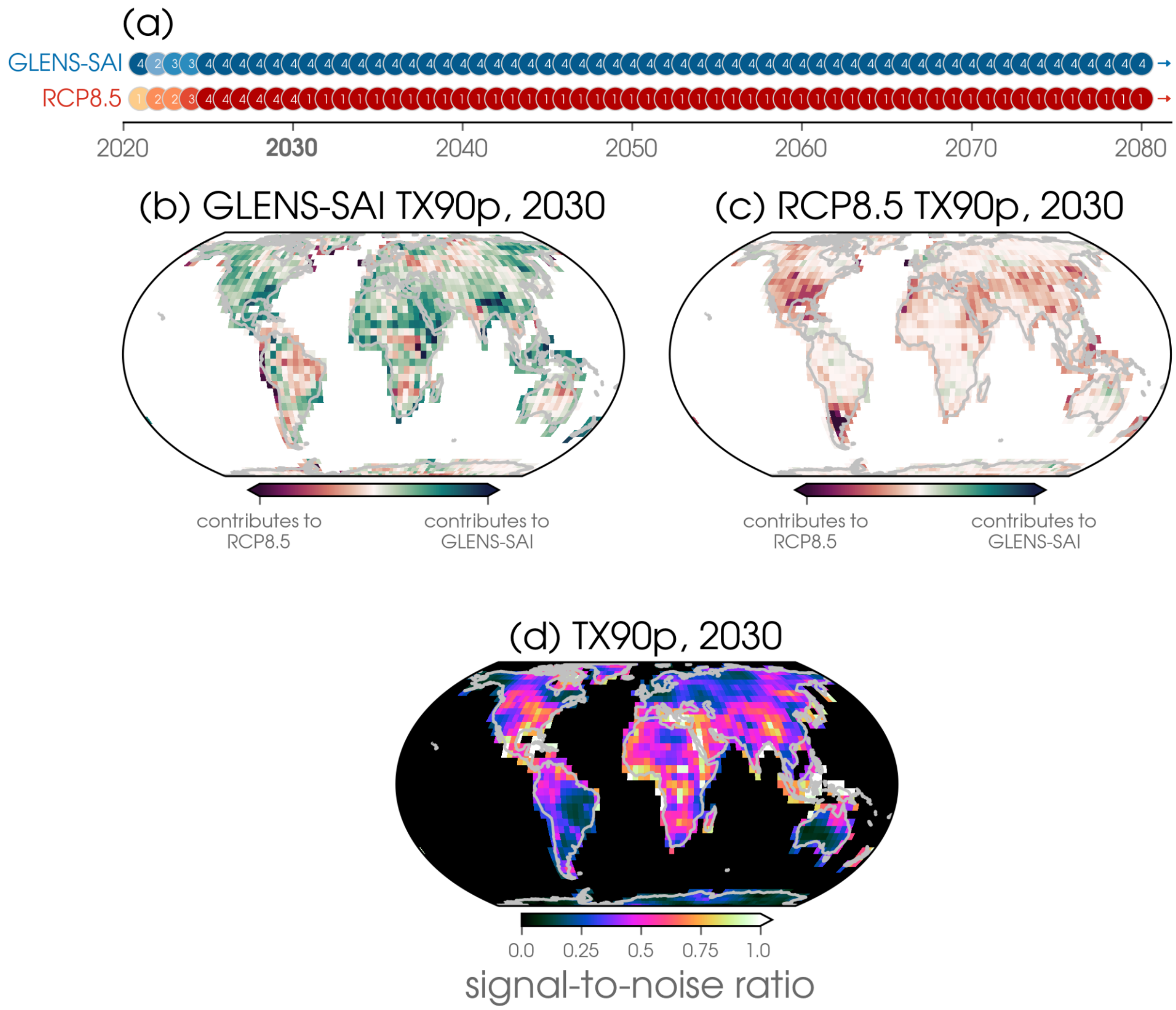

Figure 3: TX90p. (a) The number of testing samples correctly classified by the logistic regression model as a function of year. The colored shading denotes the fraction of available testing members, split into five bins from light-to-dark: 0%, 25%, 50%, 75% and 100% correct. (b) Ensemble-mean contribution across all GLENS-SAI ensemble members for the year 2030. (c) Ensemble-mean contribution across all RCP8.5 ensemble members for the year 2030. Contribution is defined as the weights*input, where positive contributions drive the logistic prediction toward one (i.e. predicting GLENS-SAI) and negative contributions drive the logistic prediction toward zero (i.e. predicting RCP8.5). (d) Signal-to-noise ratio where the signal is defined as the absolute value of the ensemble mean difference between the 20 ensemble members of the GLENS-SAI and RCP8.5 simulations. The noise is defined as the range (maximum minus minimum) of the GLENS-SAI simulations in 2030 over the 20 ensemble members.

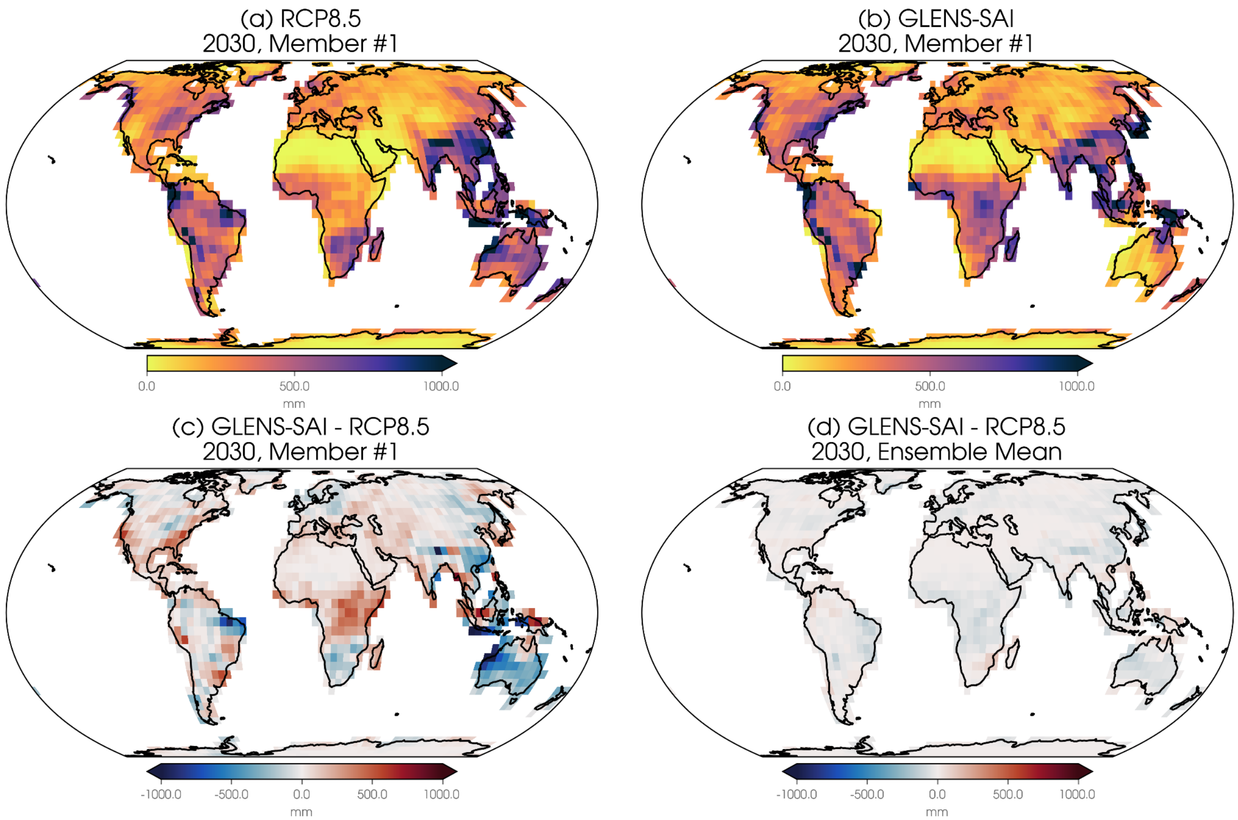

Figure 4: R95pTOT. As in Figure 2 but for extreme precipitation (R95pTOT).

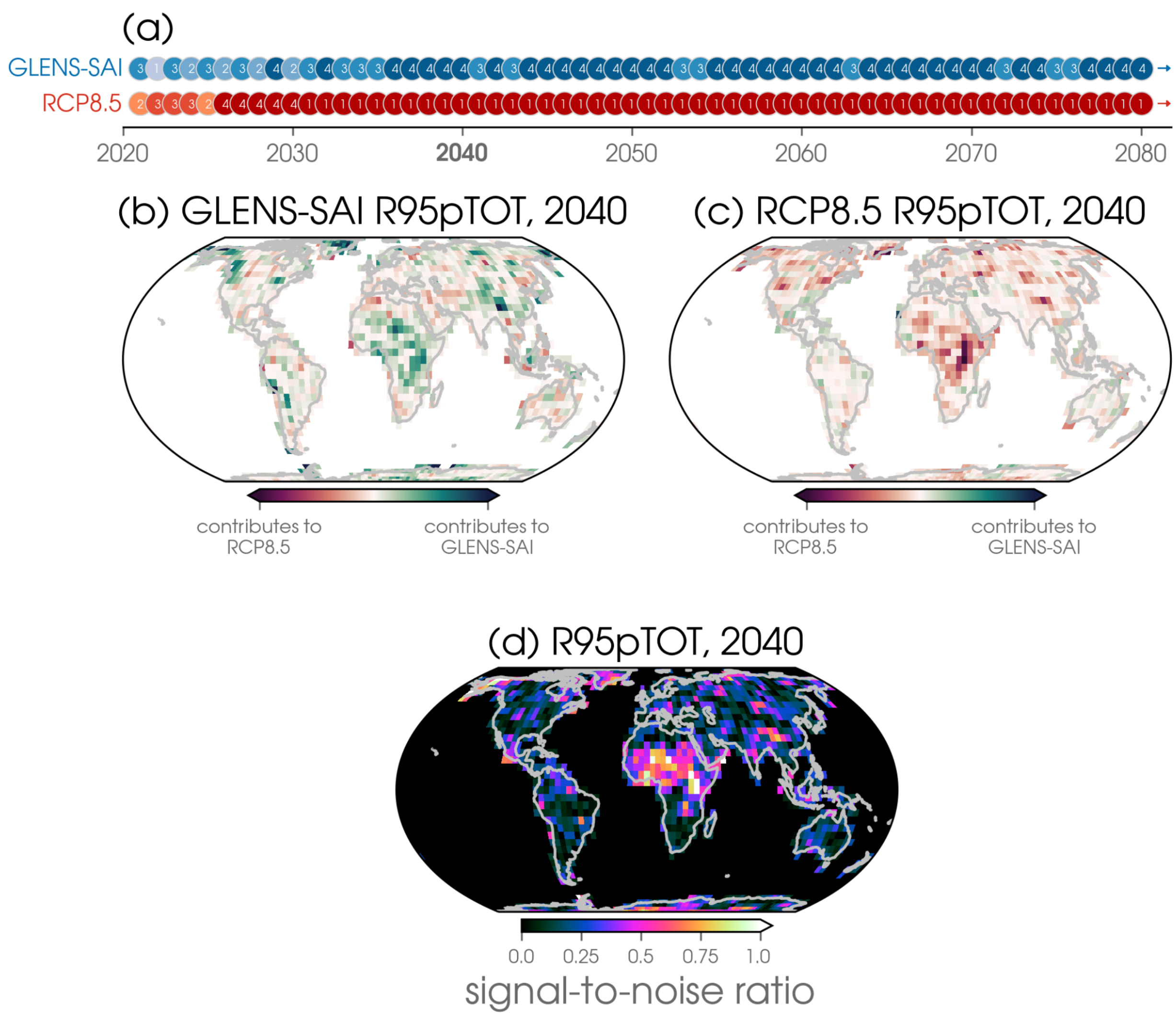

Figure 5: R95pTOT. As in Figure 3 but for extreme precipitation (R95pTOT) for 2040 in panels b-d.

SUPPLEMENTARY FIGURES
Detecting changes in global extremes under the GLENS-SAI climate intervention strategy

Elizabeth A. Barnes[1], James W. Hurrell[1] and Lantao Sun[1]

[1]Department of Atmospheric Science, Colorado State University, Fort Collins, CO

Corresponding author: Elizabeth A. Barnes (eabarnes@colostate.edu)

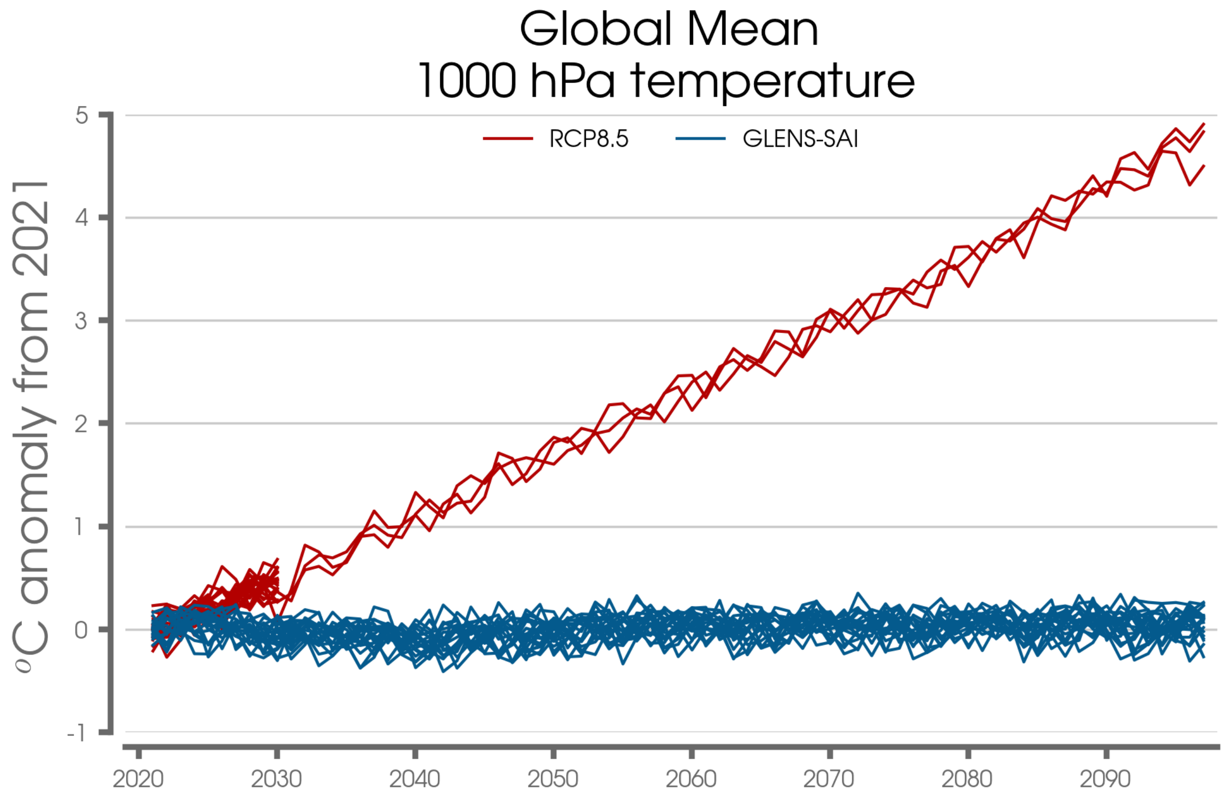

Figure S1: Global mean temperature anomaly from the 2021 ensemble mean for the RCP8.5 and GLENS-SAI ensembles.

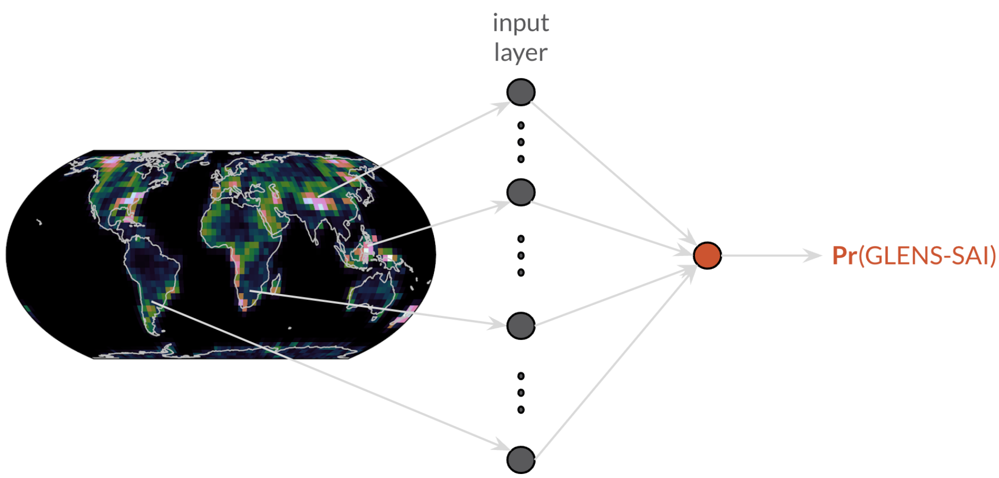

Figure S2: Logistic regression architecture.

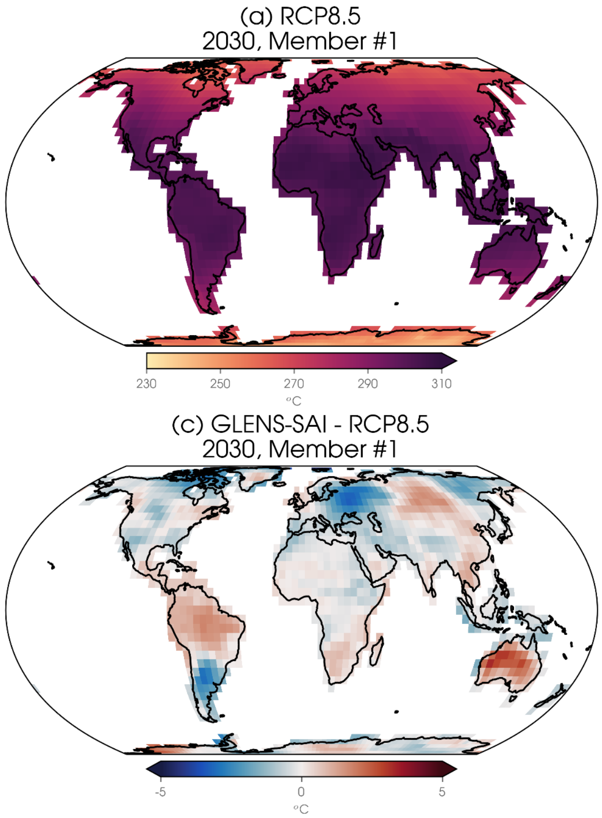

Supp. Figure S3: T. Annual mean 1000 hPa temperature in 2030 for ensemble member #1 of the (a) RCP8.5 and (b) GLENS-SAI simulations. (c) The difference in temperature between GLENS-SAI and RCP8.5 for ensemble member #1. (d) As in panel (c) but for the difference in the ensemble means (20 members for each simulation).

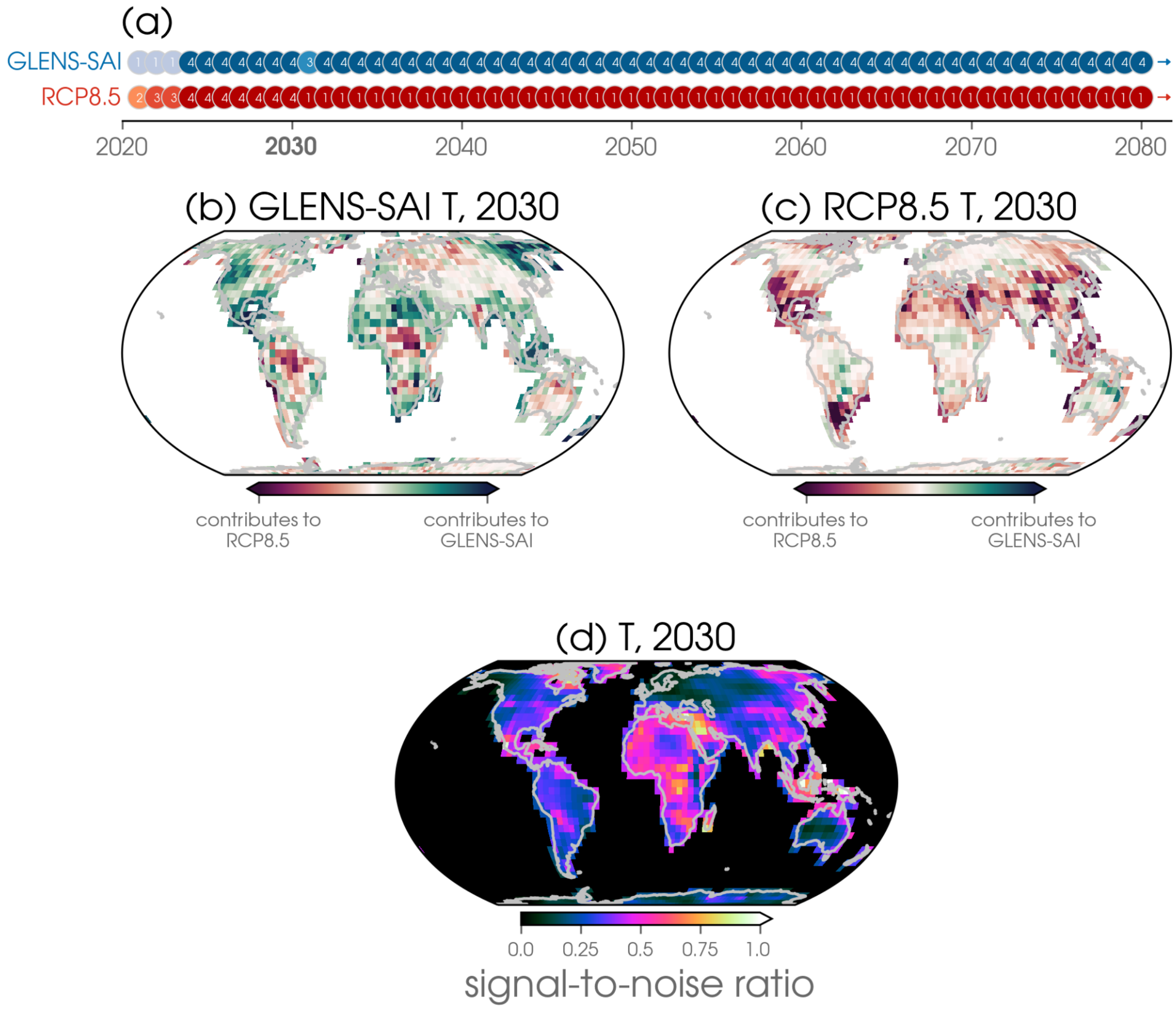

Supp. Figure S4: As in Figure 2 but for annual-mean 1000 hPa temperature.

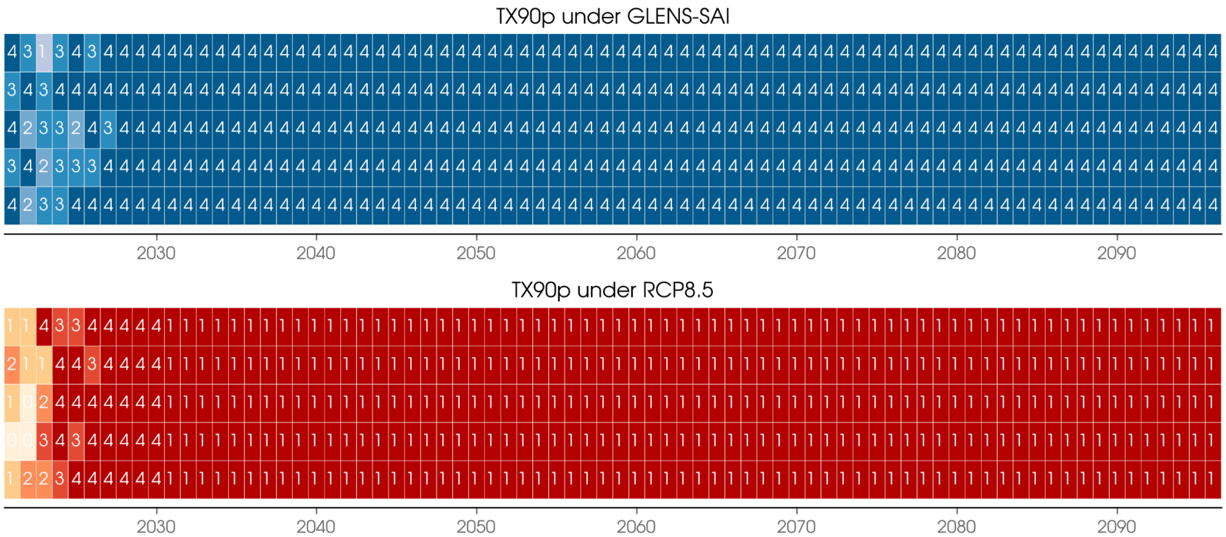

Supp. Fig. S5: Summary of model accuracy for five different logistic regression models (denoted by rows) trained using different random seeds and combinations of ensemble members for the training/testing split. The number of testing members correctly classified by the logistic regression model as a function of year is shown by white numbers. The colored shading denotes the fraction of available testing samples, split into five bins from light-to-dark: 0%, 25%, 50%, 75% and 100% correct.

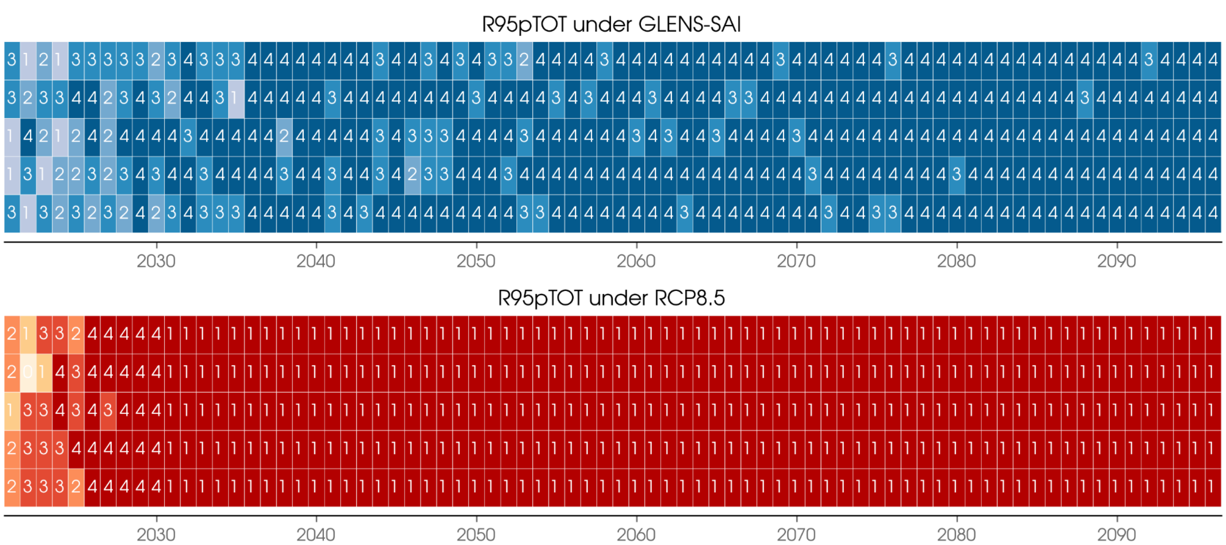

Supp. Fig. S6: As in Figure S5 but for R95pTOT.

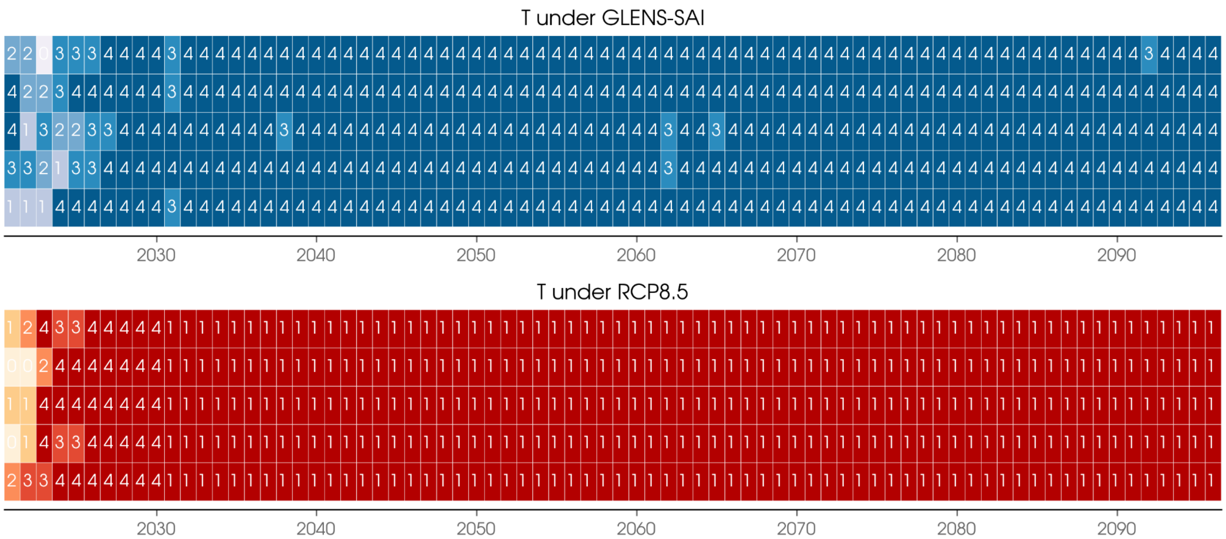

Supp. Fig. S7: As in Figure S5 but for 1000 hPa temperature.

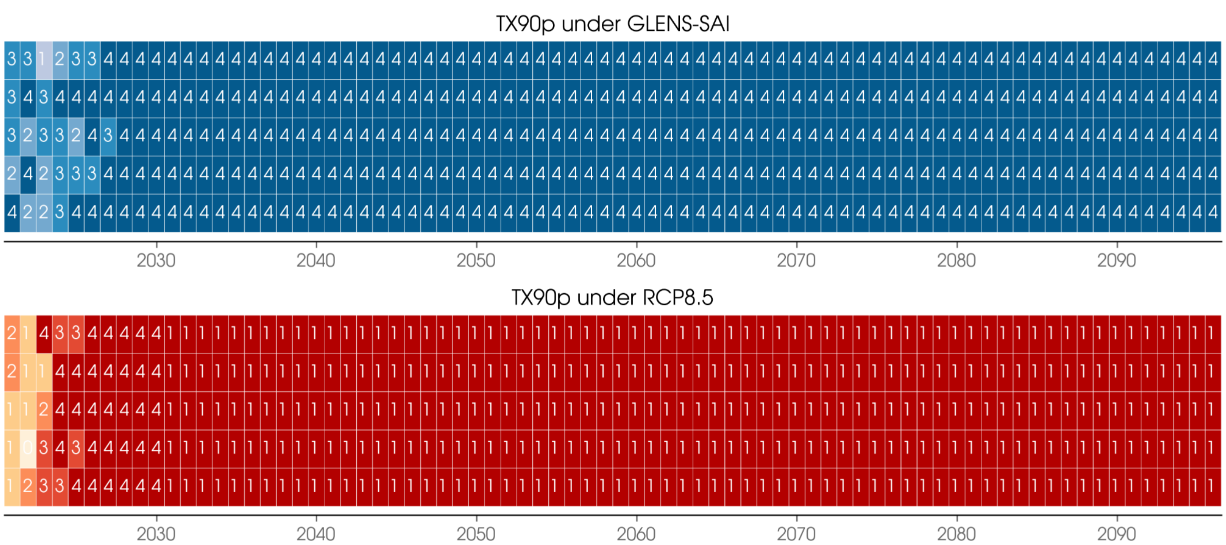

Supp. Fig. S8: As in Figure S5 using a ridge parameter of 0.0.

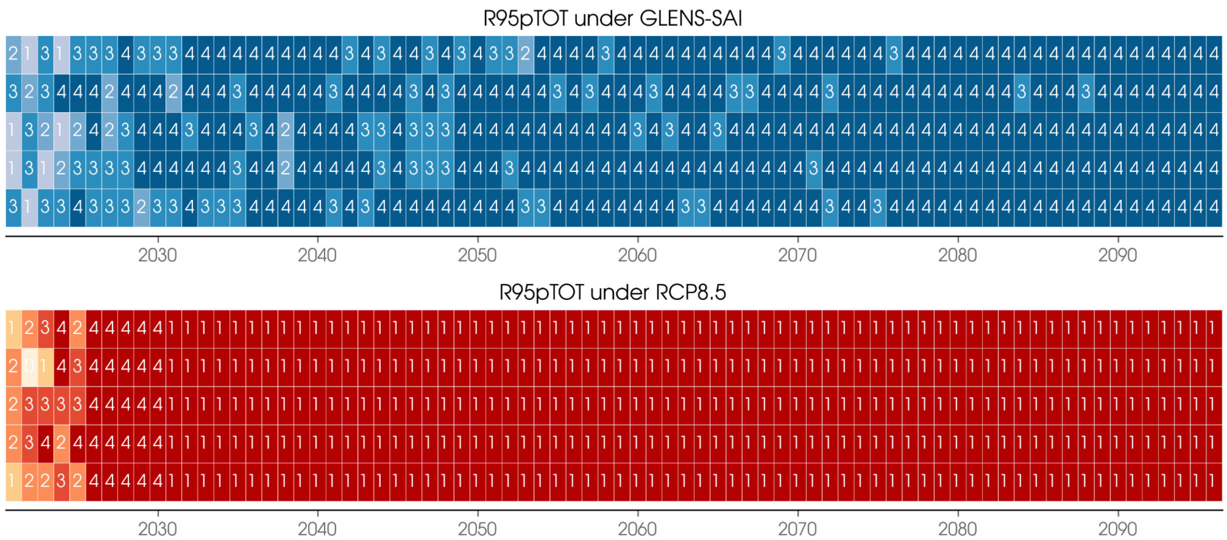

Supp. Fig. S9: As in Figure S5 but for R95pTOT using a ridge parameter of 0.0.

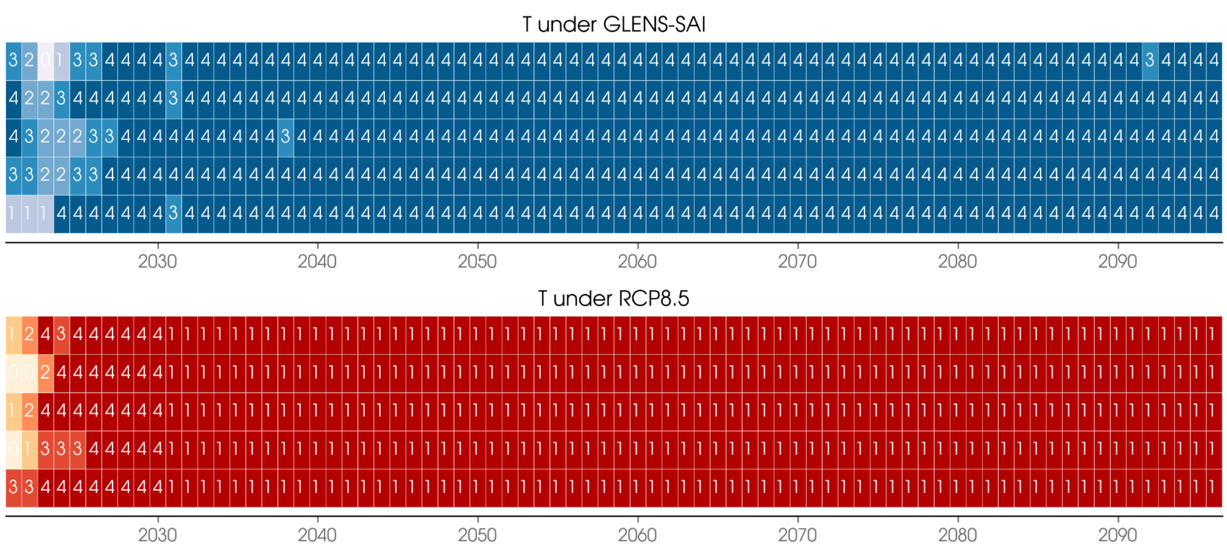

Supp. Fig. S10: As in Figure S5 but for 1000 hPa temperature using a ridge parameter of 0.0.

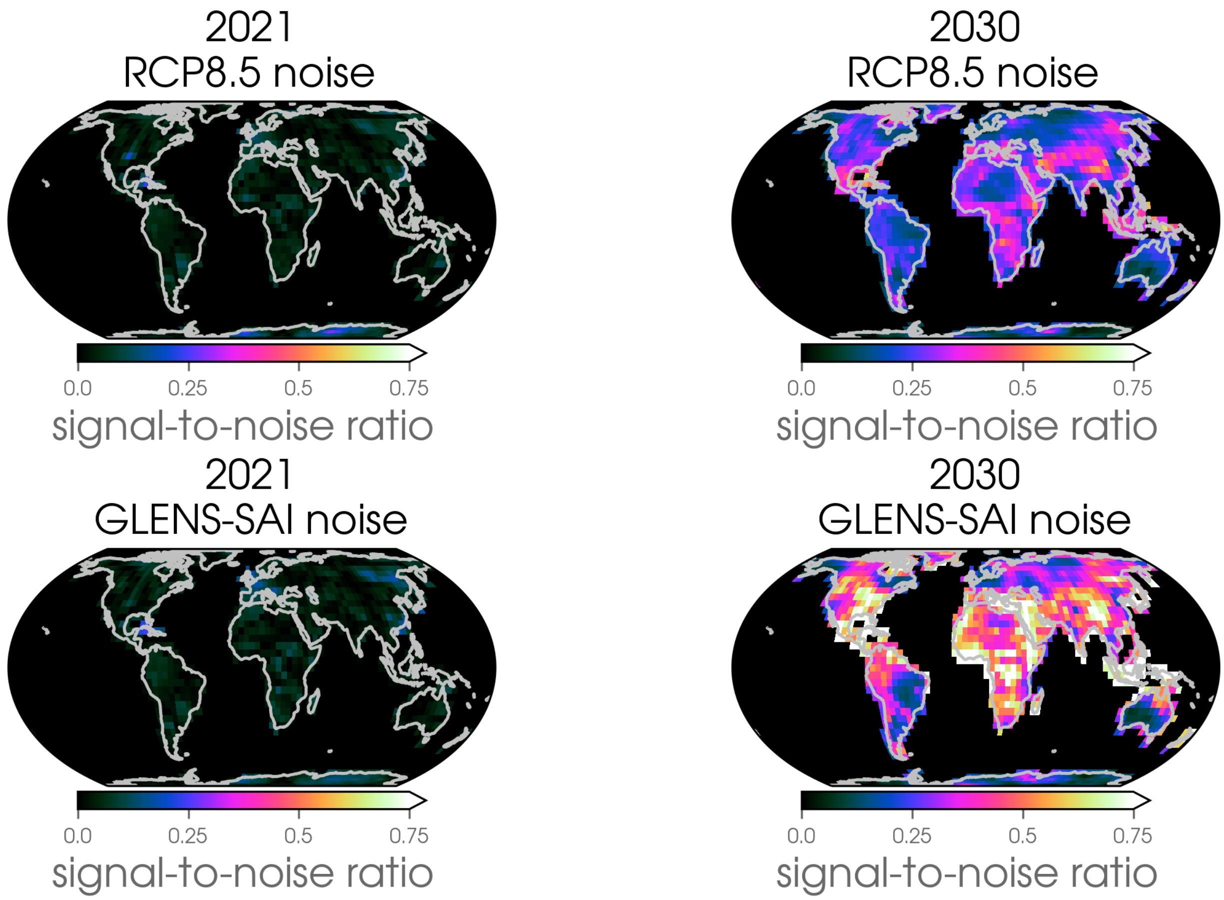

Supp. Fig. S11: Signal-to-noise ratios for TX90p where the noise is defined differently depending on the simulation used to compute the maximum minus minimum (range).

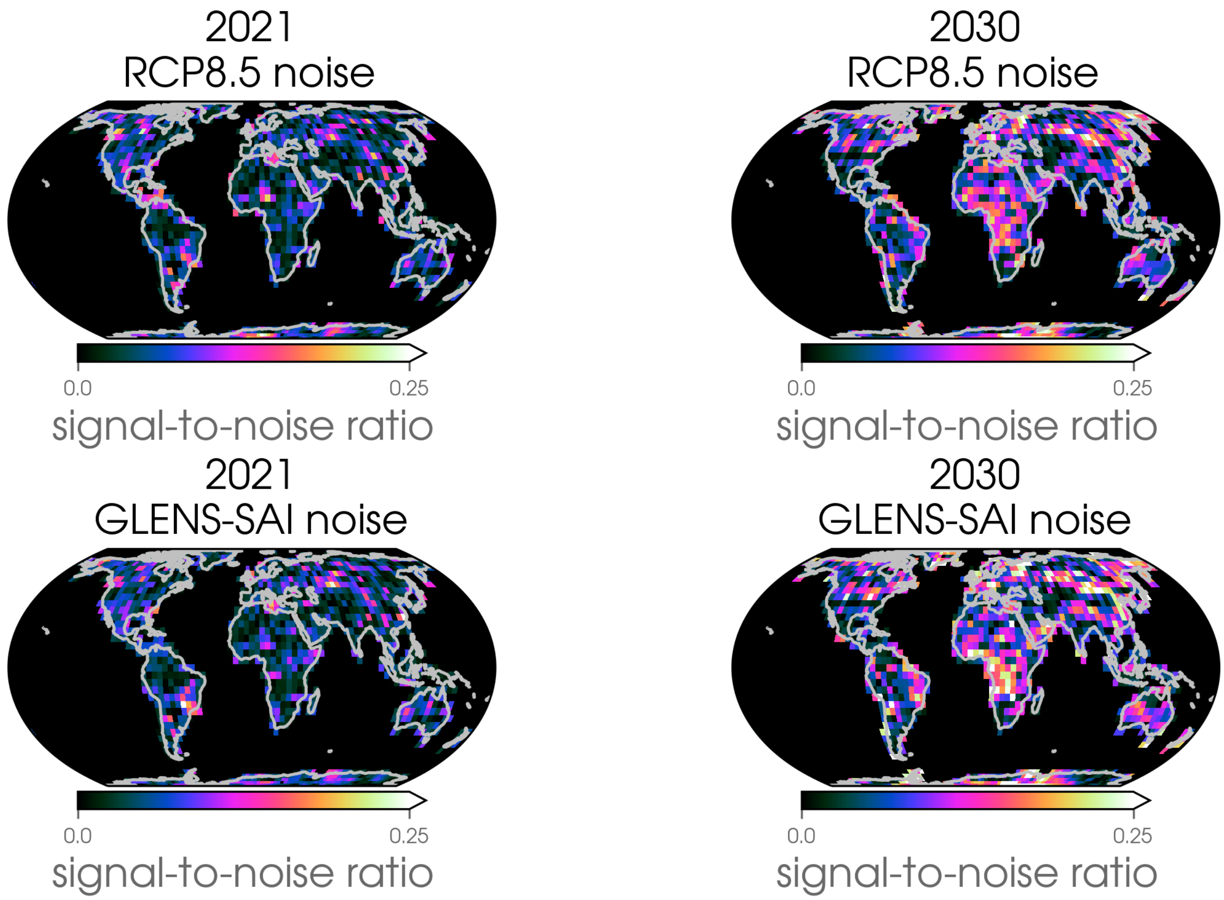

Supp. Fig. S12: As in Supp. Fig. S12 but for R95pTOT.

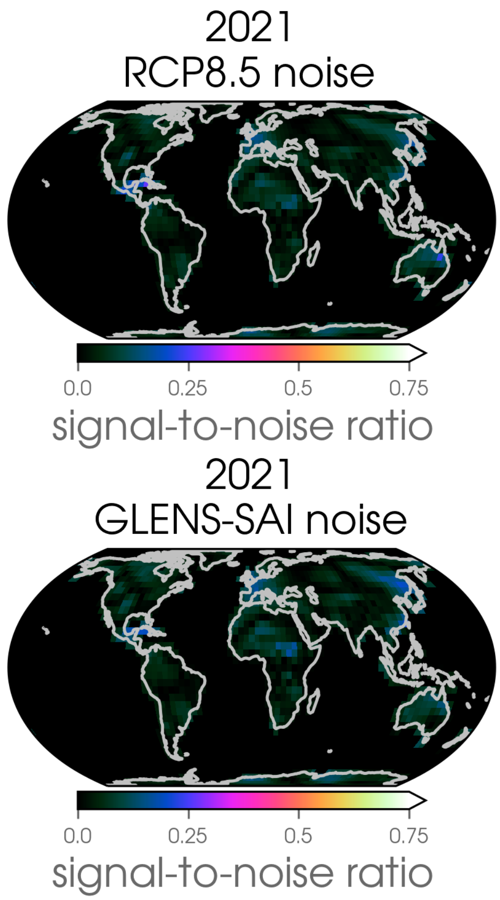

Supp. Fig. S13: As in Supp. Fig. S12 but for 1000 hPa temperature.